

REVIEW OF CENTRAL EXCLUSIVE PRODUCTION OF THE HIGGS BOSON BEYOND THE STANDARD MODEL

MAREK TAŠEVSKÝ

*Institute of Physics of the Academy of Sciences of the Czech republic,
 Na Slovance 2, 18221 Prague, Czech republic
 Marek.Tasevsky@cern.ch*

We review activities in the field of theoretical, phenomenological and experimental studies related to the production of the Higgs boson in central exclusive processes at LHC in models beyond Standard Model. Prospects in the context of the Higgs boson discovery at LHC in 2012 and of proposals to build forward proton detectors at ATLAS and CMS side are summarized.

Keywords: LHC; Higgs boson; Central exclusive production; Beyond Standard Model; Forward detectors.

PACS numbers: 13.85.-t high-energy reactions, hadrons-induced and 14.80.Bn Higgs bosons, Standard Model and 14.80.Da Supersymmetric Higgs bosons

1. Introduction

The central exclusive production (CEP) of the Higgs boson is an exciting area of research. It received a great deal of attention over the last two decades from theorists as well as experimentalists, see Refs. 1–7. The exclusivity and hence a relatively simple experimental signature makes this process unique, but the excitement perhaps arises from a question that everybody starting to explore this process has to ask: what does the exclusivity actually cost? On theory side the price is a rather low cross section. On experiment side we pay by rather low signal selection efficiencies. But the balance is put back by a favorable signal-to-background ratio. The Higgs boson with mass close to 125.5 GeV has been discovered at the LHC in 2012 by the ATLAS⁸ and CMS⁹ experiments. Preliminary studies of its properties (see for example a global analysis collecting all available LHC data in Ref. 10) suggest the Higgs boson is compatible with the Standard Model (SM), nevertheless there is still room for models of New Physics. In this review aspects of the search for the Higgs boson produced exclusively at the LHC in particular in models beyond the Standard Model (BSM) are summarized.

Theoretically this process has been discussed since the early nineties. The interest was renewed by the KMR group¹ which provided the first realistic evaluation of the expected cross section for the SM Higgs boson. For several years this process formed the core of the physics case for the FP420 project¹¹ and its offsprings AFP¹²

(ATLAS Forward Proton) in ATLAS and CT-PPS¹³ (CMS-Totem Precision Proton Spectrometer) in the CMS and Totem experiments. For various reasons the main focus of the FP420 project was installing forward proton detectors at 420 m from the interaction point (IP) from ATLAS and/or CMS, while the AFP and CT-PPS projects presently concentrate on installing forward proton detectors around 220 m. A combination of both locations is viewed as ideal, and many analyses therefore use the combined acceptance as a basis for calculations and estimates. If forward proton detectors (FPD) are installed symmetrically on the left (L) and right (R) side of the IP, the number of possible configurations amounts up to four: two symmetric ones, 420(L)+420(R) and 220(L)+220(R), and two asymmetric ones, 420(L)+220(R) and 220(L)+420(R). Although the exact positions of the AFP and CT-PPS are 210 m and 240 m, respectively, we will denote them 220 in the following. Because there are three possibilities of installation of the FPDs (stations at 220 m only, at 420 m only, and at 220 m and 420 m), the individual four configurations form three different acceptance scenarios (and hence different kinematic conditions) which will be denoted as “220” for 220(L)+220(R), “420” for 420(L)+420(R) and “total” for the sum of all four configurations.

2. Status of Proposals of Forward Proton Detectors at LHC

The physics, experimental, hardware and integration aspects studied during the R&D phase of the FP420 project were comprehensively summarized in Ref. 11. The FP420 was a collaboration of ATLAS, CMS and other groups which split into two independent projects, AFP in ATLAS and CT-PPS in CMS and Totem, which concentrate on installing stations only at around 220 m from the interaction point, IP, while considering stations at 420 m as a possible upgrade.

Designs of both the AFP and CT-PPS projects are similar. They will use 3D-Silicon tracking detectors to precisely measure the four-momentum loss of the diffractively scattered proton, ξ , and either quartz bars, gas detector or diamond sensors to measure the time-of-flight (ToF) of the deflected protons between the interaction point and the timing detectors. The ToF determines the interaction point in the beam direction if (and only if) the protons detected at opposite sides of the IP came from the same interaction, thus reducing pile-up background. Both AFP and CT-PPS (Stage I) house the detectors in Roman pots as a means of moving them very close to the beams, as in Totem experiment and ALFA (FPD in the ATLAS detector). At a later stage CT-PPS plans to use a sideways-moving beam pipe as used at PETRA collider at DESY (Hamburg). The CT-PPS project has been endorsed by the LHC Committee in September 2013; the AFP project is close to an approval by the ATLAS collaboration by the end of 2014.

3. Central Exclusive Production of Higgs boson in SM and MSSM

A comprehensive review and summary of the central exclusive production of various processes has been released recently in Ref. 14. Here we outline only the main aspects

of exclusive production.

The process is defined as $pp \rightarrow p \oplus \Phi \oplus p$ where all of the energy lost by the protons during the interaction (a few per cent) goes into the production of the central system, Φ . The final state therefore consists of a centrally produced system (e.g. dijet, heavy particle or Higgs boson) coming from a hard subprocess, two very forward protons and no other activity. The ' \oplus ' sign denotes the regions devoid of activity, often called rapidity gaps. A simultaneous detection of both forward protons and the central system opens up a window to a rich physics program covering not only exclusive but also a variety of QCD, Electroweak and BSM processes (see e.g. Refs. 3, 11–20). Such measurements can put constraints on the Higgs sector of Minimal Supersymmetric SM (MSSM) and other popular BSM scenarios.^{21–36} In the SM the CEP of Higgs bosons has been studied in Refs. 7, 15, 22, 23, 37–40.

CEP is especially attractive for three reasons: firstly, if the outgoing protons remain intact and scatter through small angles then, to a very good approximation, the primary di-gluon system obeys a $J_z = 0$, \mathcal{C} -even, \mathcal{P} -even selection rule.^{41, 42} Here J_z is the projection of the total angular momentum along the proton beam axis. This therefore allows a clean determination of the quantum numbers of any observed resonance. Thus, in principle, only a few such events are necessary to determine the quantum numbers, since the mere observation of the process establishes that the exchanged object is in the 0^{++} state. Secondly, from precise measurements of the proton momentum losses, ξ_1 and ξ_2 , and from the fact that the process is exclusive, the mass of the central system can be measured much more precisely than from the central detector, by the so-called missing mass method,² $M^2 = \xi_1 \xi_2 s$ (s is the square of the proton-proton center-of-mass energy) which is independent of the decay mode. Thirdly, in CEP, particularly for the so-far elusive $b\bar{b}$ mode, the signal-to-background (S/B) ratios turn out to be close to unity, if the contribution from pile-up is not considered. This advantageous S/B ratio is due to the combination of the $J_z = 0$ selection rule, the potentially excellent mass resolution, and the simplicity of the event signature in the central detector. Another important feature of forward proton tagging is the fact that it enables the strongest decay modes, namely $b\bar{b}$, $WW^{(*)}$, $ZZ^{(*)}$ and $\tau\tau$ to be observed in one process. In this way, it may be possible to access the Higgs boson coupling to bottom quarks. This may be challenging in conventional search channels at LHC due to large QCD backgrounds, even though $h \rightarrow b\bar{b}$ is the dominant decay mode for a light SM Higgs boson. Here it should be kept in mind that access to the bottom Yukawa coupling will be crucial as an input also for the determination of Higgs couplings to other particles.^{43–46}

The last few years witnessed a fair development in the calculations of the CEP cross sections concerning both the hard matrix element (see Refs. 4, 47–55) and the so-called soft absorptive corrections and soft-hard factorization breaking effects (see Refs. 56, 57 for details and references). There are basically four groups providing calculations of the cross-sections for the CEP of the SM Higgs boson, whose most recent predictions are in Refs. 7, 52–55. Their approaches differ in a number of aspects (e.g. different soft survival probabilities, different scales in the Sudakov

derivative or even its complete absence). Predictions differ within the same group, depending on input parameters, e.g. parton density functions (PDF), but if taken globally, predictions of all four groups range between roughly 0.5 fb and 2 fb, leading to an uncertainty factor of three which is much progress compared to a situation in the previous decade. Since the KMR calculations i) successfully describe existing data, ii) are maintained and improved and iii) form a basis of all analyses reviewed in this document, we briefly summarise the recent development, while a complete review can be found in Ref. 14. Calculations of the combined enhanced- and eikonal-soft survival factor give lower values than the value 0.03 used in several analyses, e.g. in Refs. 22–25,39. Also taking a more appropriate factorization scale M (rather than $\approx 0.62M$) in calculating Sudakov suppression almost halves the CEP cross section (of both the signal and the background).⁴⁸ On the other hand as discussed in^{58,59} we may expect the cross section to be increased by higher order corrections and by using the CTEQ6L⁶⁰ Leading Order (LO) proton PDF that give the best agreement of the CEP calculations with CDF data on exclusive $\gamma\gamma$ production.⁶¹ The combined effect of all changes is estimated to be rather small. Ways to test the theoretical formalism at LHC, with or without forward proton tagging, are summarized in Ref. 62.

3.1. $H \rightarrow b\bar{b}$

There are three independent analyses which have been studying the feasibility and significance of the CEP Higgs boson decaying into $b\bar{b}$ in the SM. They have all arrived at an almost identical set of cuts to select the signal and suppress all types of background. In Ref. 15 experimental efficiencies have been obtained in the range of masses between 100 and 300 GeV using a fast CMS simulation, in Ref. 39 results for one mass point of 120 GeV were based on a fast ATLAS simulation and in Ref. 22 one mass point at 120 GeV has been studied using generator-level quantities that have been smeared using resolutions published in the ATLAS TDR.⁶³ After applying all these cuts, the numbers of events for the signal, for the irreducible backgrounds (defined as coming from the CEP and Double Pomeron Exchange (DPE) processes) and for the overlap backgrounds (defined later) obtained at the mass of 120 GeV are very similar among the three analyses, with the exception of Ref. 15 where the overlap background numbers are higher due to not applying a cut on the number of charged tracks outside the dijet system (see later). The numbers of CEP signal and background events are estimated by ExHuMe MC event generator,⁶⁴ the DPE background by Pomwig⁶⁵ and the overlap backgrounds by Pythia⁶⁶ or Herwig.⁶⁷ For an integrated luminosity of 30 fb^{-1} and for the FPDs at 420 m and total acceptance scenarios separately, they amount to 2 and 3 for the signal, 3 and 4 for the CEP backgrounds and are negligible for the DPE backgrounds. The remaining overlap backgrounds depend non-linearly on the instantaneous luminosity and they were estimated to be negligible at luminosity of $10^{33} \text{ cm}^{-2} \text{ s}^{-1}$, while they amount to roughly 20 and 40 events at luminosity of $10^{34} \text{ cm}^{-2} \text{ s}^{-1}$ for the two FPD accep-

tance scenarios. Significances coming from these signal and background numbers are moderate and they would have to be improved to attain more favorable prospects. Ways to improve these significances are discussed in Refs. 22, 25. For example we can surely expect improvements in the gluon-jet/ b -jet mis-identification probability $P_{g/b}$. In the original analyses in Refs. 22–25, 39 a conservative approach has been followed by taking the maximum of two values available at that time in ATLAS and CMS, which was $P_{g/b} = 1.3\%$ used in ATLAS. Meanwhile new developments were reported in reducing the light-quark- b mis-identification probabilities in ATLAS⁶⁸ and CMS.⁶⁹ Other possibilities to improve the significances in searching for the SM Higgs in CEP are a possible sub-10 ps resolution for timing detectors, the use of multivariate techniques or a further fine-tuning or optimization of the signal selection and background rejection cuts, thanks to the fact that the mass of the SM-like Higgs boson is already known with a relatively high precision. The known Higgs boson mass can also greatly facilitate proposals for a dedicated L1 trigger to efficiently save events with the CEP $H \rightarrow b\bar{b}$ candidates. Proposals made in Ref. 70, well before the SM-like Higgs boson discovery, can thus be further optimized.

3.1.1. *Pile-up effects*

At luminosities greater than $10^{33} \text{ cm}^{-2} \text{ s}^{-1}$, high energy interactions are accompanied by a number of soft interactions in the same bunch-crossing, so called pile-up events. The most dangerous combination arises from an overlap of a non-diffractive (ND) event with a hard scale (e.g. a dijet event with jet transverse momentum as the hard scale in the case we are searching for the $H \rightarrow b\bar{b}$ signal) with two additional Single Diffractive (SD) events each having a leading proton inside the acceptance of FPDs. The overlap of these three events can resemble a signal event and is the most prominent source of background in this channel at high instantaneous luminosity (around $10^{34} \text{ cm}^{-2} \text{ s}^{-1}$). At low instantaneous luminosity (around $10^{33} \text{ cm}^{-2} \text{ s}^{-1}$), the overlap background is at a per-mil level and the CEP backgrounds dominate (numbers are given in the previous subsection).

In all three analyses in Refs. 15, 22, 39 the quantitative effect of overlaid pile-up events was assessed for the signal sample, for the diffractive background sources and for the ND $b\bar{b}$ dijet background. It was studied by mixing, event-by-event, a certain number of minimum bias events with one signal or one background event. This number is determined from Poisson statistics; it depends linearly on luminosity and is model-dependent since the total pp cross section at $\sqrt{s} = 14 \text{ TeV}$ has not yet been measured. The effect of the overlap background is quantified by a process-independent probability of a fake double-proton tag, i.e. of detecting two protons in FPDs, each on opposite sides of the IP, caused by outgoing protons from pile-up events. The results are summarized in Refs. 22, 39, here only the main facts are summarized.

At a luminosity of $10^{33} \text{ cm}^{-2} \text{ s}^{-1}$, where the average number of pile-up events per bunch crossing is 3.5 (including elastic events), the probability of an event to

have a fake double-proton tag caused by pile-up protons is a few per-mil for all three FPD configurations. At $\mathcal{L} \sim 10^{34} \text{ cm}^{-2} \text{ s}^{-1}$, where the average number of pile-up events per bunch crossing is 35 (including elastics), the probabilities reach 7%, 21% and 23% for the 420+420, 220+220 and 420+220 configurations, respectively, for assumed distances from the beam center of 2.5 mm at 220 m, and 4 mm at 420 m including a dead zone of 1 mm.

The numbers of fake proton pairs per bunch crossing, N/BX , as a function of the number of pile-up events per bunch crossing, N^{PU} , is purely combinatorial and well described by the following formula:³⁹

$$N/BX = 2e^{-\mu_{\text{SS}}}(\cosh(\mu_{\text{SS}}) - 1) + 1 - e^{-\mu_{\text{DS}}} \quad (1)$$

Here $\mu_{\text{SS}} = A_{\text{SS}} * N^{\text{PU}}$ and $\mu_{\text{DS}} = A_{\text{DS}} * N^{\text{PU}}$ denote the probability to see pile-up protons in the FPDs on one side only (“SS”, single-sided) and on both sides (“DS”, double-sided), respectively. As is evident from the formula, the number N/BX crucially depends on the probability A_{SS} . There are several estimates of this probability for FPDs at both, 420 m and 220 m available in literature which can be compared. In Ref. 39 a high statistics Pythia sample of minimum bias events and 2-dimensional (ξ, p_T) -FPD acceptances gave 0.9% and 1.7% for A_{SS} at 420 m and 220 m, respectively, and negligible numbers for A_{DS} at both, 420 m and 220 m. The latter fact is due to the absence of the DPE processes in Pythia. In Ref. 22 only basic cuts $0.005 < \xi_1 < 0.018$, $0.004 < \xi_2 < 0.014$ and $0.02 < \xi < 0.2$ were used as rough estimates of the 420 and 220 acceptances, respectively, and for these, 1.1% and 2.4% were obtained with PYTHIA 6.4, while 1.2% and 3.1% were reached by PHOJET 1.2. In Ref. 15 where the distances of the active region of the detectors were 1.5 mm and 4.5 mm for the 220 and 420 stations, respectively, and 2-dimensional (ξ, p_T) -FPD acceptances and PHOJET 1.2 were used, the probabilities of 1.0% and 3.1% were reported. Finally, a theoretical estimate was made based on a model with a complete set of multi-Pomeron vertices. This model is described in Ref. 71, where it is shown to be consistent with the HERA data on the triple-Pomeron vertex, and the estimates were based on the same basic ξ cuts as used in Ref. 22 are 1.0% and 2.5%. These numbers critically depend on the normalization of the leading proton ξ spectrum, which has not yet been measured at $\sqrt{s} = 14$ TeV for which the above estimates are given.

At $\sqrt{s} = 14$ TeV, cross-sections of soft SD events or ND dijet events with $p_T > 30$ GeV range around 10 mb or tens of μb , respectively, so reducing such huge backgrounds down to a tolerable level, comparable or smaller than the cross section of the signal after applying all the stringent cuts, is a real challenge.

All signal selection and background rejection cuts are described in Refs. 15,22,39. As an example, in Fig. 1 we show two quantities that provide an excellent separation between the signal and the overlap background and are thus used to significantly suppress the overlap background.

The $|\Delta y|$ variable is defined as a difference between pseudorapidity of the central system calculated from the central detector and from the FPD, the latter based on

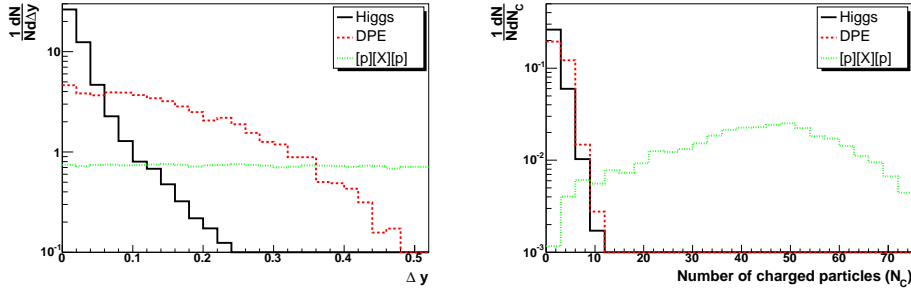


Fig. 1. The $|\Delta y|$ (left) and N_c (right) distributions are shown for the signal, DPE and overlap backgrounds. Events were generated by the ExHuMe MC event generator with momenta of particles smeared with ATLAS detector resolutions, and use the cone jet algorithm with a cone radius of 0.7. Taken from Ref. 22.

the precise measurements of ξ . The N_c variable is a number of charged particles outside the dijet system and thus gives an estimate of the number of charged particles not associated with the hard-scale process. The multiplicity difference for the signal and overlap background can then be accounted for by two facts: firstly the central system in non-diffractive events is color-connected with proton remnants, therefore the total number of produced particles is higher than that in a diffractive event. Secondly, basically for the same reason, the underlying event producing soft particles may be present in the non-diffractive event, while it is believed to be significantly suppressed in the diffractive event.

Another very powerful means to suppress the overlap background is exploiting fast timing detectors whose goal is to distinguish whether the proton detected in a FPD originates from a hard-scale event or from a pile-up event. The ToF difference between the two protons gives the z -position of the collision, to match with the central event. Fast timing detectors with an expected resolution of around 10 ps and hence z -resolution ~ 2 mm are part of the AFP and CT-PPS projects. Monte Carlo studies^{22,39} suggest that with nominal running conditions a fair rejection is possible of events with fake protons. If a $2\sigma_t$ cut (σ_t is resolution of the ToF detector) is applied on the time measurement, the rejection is 19 (18, 16 and 15) at an instantaneous luminosity of 1 (2 , 5 and 10) $\times 10^{33} \text{ cm}^{-2} \text{ s}^{-1}$, respectively.

3.1.2. BSM scenarios

Numerous models of new physics require an extended Higgs sector. A frequently used extension of the SM is the MSSM,^{72–74} where the Higgs sector consists of five physical states (two Higgs doublets are required). At the lowest order the MSSM Higgs sector is \mathcal{CP} -conserving, containing two \mathcal{CP} -even bosons, the lighter h and the heavier H , a \mathcal{CP} -odd boson, A , and the charged bosons H^\pm . It can be specified in terms of the gauge couplings, the ratio of the two vacuum expectation values, $\tan\beta \equiv v_2/v_1$, and the mass of the A boson, M_A . The Higgs sector of the MSSM is

affected by large higher-order corrections (see for example Refs. 75–77 for reviews), which have to be taken into account for reliable phenomenological predictions.

In the last decade, detailed analyses of the CEP of the Higgs boson in MSSM have been presented in four basic papers 22–25. Results of Refs. 23–25 are based on the same set of experimental acceptances and efficiencies, namely that discussed in Ref. 15, and the evolution between the results of Ref. 23 and Ref. 25 is described later. Since results in Ref. 22 and Refs. 23–25 are based on independent analyses, here we briefly outline the main differences in approaches and compare results where possible. The differences are as follows:

- (i) FPD ACCEPTANCES. The results in Ref. 22 are based on the ATLAS detector and FPD acceptances at the ATLAS side of the IP, while the results in Refs. 23–25 are based on the CMS acceptances. A non-negligible difference in the FPD acceptances is observed for the asymmetric 420+220 configuration where the acceptance at CMS side is lower by roughly 30% than that at ATLAS side, if the same distances from the beam center are considered. This is caused by the horizontal (rather than vertical) plane of the crossing angle of the beams at CMS IP.
- (ii) DECAY MODES. In Ref. 22 only the $b\bar{b}$ decay mode is studied, while in Refs. 23–25 all three main decay modes, namely $b\bar{b}$, WW and $\tau\tau$ are studied.
- (iii) L1 TRIGGERS. In Ref. 22, three L1 triggers are considered for the symmetric 420+420 configurations, while for the asymmetric 420+220 configuration, a L1 trigger based on the information from the FPD at 220 m is used and this trigger is assumed to be fully efficient. The first L1 trigger for the symmetric FPD events is a low p_T muon trigger of 6 GeV in addition to a 40 GeV jet. The second is a rapidity gap trigger where gaps would be defined by requiring a veto in very forward detectors (such as ZDC and LUCID in ATLAS or ZDC, CASTOR and Totem T1 and T2 telescopes on the CMS side). This trigger requires low luminosities - the trigger efficiency is estimated to be $\sim 17\%$ at $10^{33} \text{ cm}^{-2} \text{ s}^{-1}$ and $\sim 2\%$ at $2 \times 10^{33} \text{ cm}^{-2} \text{ s}^{-1}$. The third trigger allows a high, fixed L1 rate for 40 GeV jets which is then substantially reduced at L2 by utilizing information from stations at 420 m. The L1 rates of 25 kHz and 40 kHz are examined. In Ref. 23 any of the following four L1 triggers can be used. The first takes the signal in one of the stations at 220 m and at least two jets with $p_T > 40$ GeV. As was shown in Ref. 78, for this trigger a tolerable L1 bandwidth of 1 kHz may be kept only up to luminosities of about $\mathcal{L} \sim 2 \times 10^{33} \text{ cm}^{-2} \text{ s}^{-1}$ due to the overlap background. The second trigger requires a jet with $p_T > 40$ GeV and one muon with $p_T > 3$ GeV, both measured in the central detector. The third trigger requires at least two jets with $p_T > 90$ GeV in the central detector, so this trigger is useful only for high-mass searches. The fourth trigger, requiring electrons or muons in the central detector, is focused on retaining mainly events with W bosons decaying leptonically or semileptonically. While corresponding cuts are used at analysis level to mimic the triggers, they are assumed to be fully

efficient.

- (iv) **BACKGROUND TREATMENT.** As stated in the previous item, the two analyses only overlap in the $b\bar{b}$ decay mode, therefore the background treatment can only be compared for this decay mode. In Ref. 23 background sources of the WW and $\tau\tau$ decay modes are also carefully discussed and these are summarised in separate subsections below. In both analyses, the same sources of background are considered for the $b\bar{b}$ decay mode, namely CEP $gg \rightarrow gg/b\bar{b}$, DPE $gg \rightarrow b\bar{b}$ and overlap backgrounds coming from an overlap of a hard scale event with pile-up events.
 - (a) *Non-overlap backgrounds.* In Ref. 22, the contributions of the above sources of background are estimated using the LO MC event generators, namely ExHuMe for the exclusive processes and Pomwig with the H1 diffractive PDFs (so called H1 2006 DPDF Fit B) for DPE processes. In Refs. 23–25 the background contributions are calculated analytically for the CEP and DPE processes including higher-order contributions and the following four most prolific sources of the CEP background have been considered in : i) LO $gg \rightarrow gg$ where gluons may be misidentified as b-jets. Note that here a conservative value of $P_{g/b} = 1.3\%$ has been used for this misidentification probability. ii) An admixture of $|J_z| = 2$ production, arising from non-forward going protons, which contributes to the LO $gg \rightarrow b\bar{b}$ background. iii) Since the b-quarks have non-zero mass there is a contribution to the $J_z = 0$ cross section of the order of m_b^2/E_T^2 . iv) Finally the NLO $gg \rightarrow b\bar{b}g$ contribution which for hard gluon radiation at large angles does not obey the selection rules. The latest results^{79,80} suppressing the contribution in the LO by a factor of roughly two are included in the calculation of the total background cross section in the point iv. To suppress the contribution of the DPE $gg \rightarrow b\bar{b}$ background, an additional cut on the polar angle of b-jets in the $b\bar{b}$ rest frame, $60^\circ < \theta < 120^\circ$, has been imposed after which this background has been estimated to be very small, as confirmed in Ref. 22 by using the LO Pomwig generator.
 - (b) *Overlap background.* The effect of the overlap background has been elaborated in Ref. 22, while in Refs. 23–25 the overlap background is considered to be negligible after applying all stringent cuts to suppress this background. As summarised above, at luminosities around $10^{33} \text{ cm}^{-2} \text{ s}^{-1}$, the overlap background may be neglected, however, by neglecting this background at luminosities $10^{34} \text{ cm}^{-2} \text{ s}^{-1}$, one anticipates a fair improvement in selecting signal as well as in taming this background. There are definitely ways to improve significances and they were discussed above.
- (v) **MSSM PARAMETER SPACE.** In Ref. 22 one example point is examined, namely the $(\tan \beta, M_A) = (40, 120 \text{ GeV})$, while in Refs. 23–25 a full scan over the MSSM parameter space $(\tan \beta, M_A) = (2\text{--}50, 100\text{--}300 \text{ GeV})$ is performed.
- (vi) **MSSM BENCHMARK SCENARIOS.** In Ref. 22 the above example point is studied in the Mhmax scenario, while in Ref. 23 two benchmark scenarios are examined

for the $b\bar{b}$ decay mode, namely the Mhmax and no-mixing scenarios. In Ref. 24, 25 a number of other scenarios have been investigated and they will be described later. We note that in Ref. 23 the Mhmax and no-mixing scenarios were also used for the $\tau\tau$ decay mode, while for the WW decay mode the small α_{eff} scenario is used as the one where the enhancement of signal cross sections is highest.

A comparison of the two independent analyses (described in Refs. 22, 23) has been performed in Ref. 11 for the only point in the MSSM parameter space that has been studied in Ref. 22, namely at $(\tan\beta, M_A) = (40, 120 \text{ GeV})$ and a good agreement has been found at luminosities where pile-up is not an issue (i.e. smaller than $2 \times 10^{33} \text{ cm}^{-2} \text{ s}^{-1}$). A comparison we make here shows a qualitative agreement also at high luminosities ($10^{34} \text{ cm}^{-2} \text{ s}^{-1}$), if similar conditions are used to analyse the signal and backgrounds. Both analyses use very similar cuts to select the signal and to suppress the backgrounds. If also similar FPD acceptances are used, very similar signal selection efficiencies can be achieved. In Ref. 22 FPD acceptances are provided for several options of the distance of the detector from the beam center, therefore for this comparison we have chosen the option which gives the closest FPD acceptances to those used in Refs. 23–25 (all FPD configurations are used). Concerning backgrounds, on the one hand, as explained above, the overlap background is not zero even after applying all stringent suppressing cuts. On the other hand, the differences in the non-overlap background treatment summarised above have not been fully evaluated, nevertheless, rough estimates show that the irreducible backgrounds in Refs. 23–25 turn out to be higher than in Ref. 22 because more effects are included than in the LO ExhuMe program, so in the end the deficit of remaining background in Refs. 23–25 is partly compensated. If finally the L1 triggers are assumed to be fully efficient, both analyses yield significances well above 5σ for the studied point $(\tan\beta, M_A) = (40, 120 \text{ GeV})$ at any instantaneous luminosity, as observed in Fig. 2 top in Ref. 24, which is to be compared with Figs. 15 and 17 b) in Ref. 22).

The results presented in Refs. 23–25 show an evolution in time which can briefly be summarised as follows. The results from Ref. 23 have already been described above. In Ref. 24, 25 the actual version of the code **FeynHiggs**^{81–85} was always employed for the MSSM cross section and decay width calculations and of the code **HiggsBounds**^{86, 87} for the evaluation of the exclusion regions corresponding to searches for MSSM Higgs bosons at LEP, Tevatron and LHC. After Ref. 24 more accurate calculations were taken of the process associated with bottom-mass terms in the Born amplitude contributing to the total background of the $b\bar{b}$ mode.^{79, 80} Besides the M_h^{max} and no-mixing scenarios other scenarios have been investigated, namely in Ref. 24 those yielding the correct amount of the cold dark matter abundance, the so-called Cold Dark Matter (CDM) scenarios (see Refs. 88, 89 for more details), and another model beyond the SM, the so-called SM4 model (see e.g. Ref. 90) with a fourth generation of quarks and leptons. While the SM4 model is practically ruled out⁹¹ by the recent LHC measurements of Higgs-mediated cross

sections^{92,93} and direct searches,^{94,95} the CDM scenarios are still viable. In Ref. 25, concentrating on the $b\bar{b}$ decay mode, seven other new benchmark scenarios have been investigated, all compatible with the mass and production rates of the observed Higgs boson signal at 125.5 GeV and all recently proposed in Ref. 96. The scenario with the best prospects for observing the CEP $H \rightarrow b\bar{b}$ process in the MSSM is the so-called low-MH scenario shown in Fig. 2. In the allowed region (the green area in Fig. 2) which is given by the combined experimental and theoretical uncertainties on the Higgs boson mass (see Ref. 97 for more details about the theory uncertainties), significances of at least 3σ are obtained for light Higgs boson masses around 80–90 GeV. This is a mass region which is slightly more challenging than that so far studied around 120 GeV (see more discussion in Ref. 25). We note that this region of interest may be ruled out by recent ATLAS searches for the light charged Higgs boson⁹⁸ which could not be considered in Ref. 25. However a dedicated analysis of the exclusion bounds in this scenario, including the CMS results, still needs to be carried out. We conclude that although room for a comparatively low mass (below 200 GeV) BSM Higgs boson is decreasing, the heavy BSM Higgs bosons cannot be entirely excluded.

Refs. 24, 25 also stress the importance and advantages of the CEP process in determining the spin-parity quantum numbers of Higgs bosons, and also in searching for a possible \mathcal{CP} -violating signal in the Higgs sector.⁹⁹

3.2. $H \rightarrow WW^{(*)}$

This channel does not suffer from any of the difficulties present in the $b\bar{b}$ channel: suppression of the dominant backgrounds does not rely primarily on the mass resolution of the FPDs, background cross sections are calculated with a sufficient precision and probably, in the leptonic and semi-leptonic decay modes, standard L1 leptonic triggers may be used. From experimental point of view, there are three main categories of events with two W bosons in the final state.

- (1) **Fully leptonic.** Events in which both W bosons decay into either an e or a μ are the simplest and will typically pass the L1 trigger thresholds due to the high p_T final state lepton. A portion of the events with decays into one or two τ 's will pass the L1 trigger thresholds with τ subsequently decaying leptonically. The inclusive branching ratio (with decays either into e or μ or τ) is 10.3%.
- (2) **Semi-leptonic.** Events in which one W boson decays leptonically and the other into two jets can be triggered by the leptonic L1 triggers mentioned in the item above. The branching ratio for cases when one W boson decays into one of the lepton types and the other W boson into two jets is about 14.5%, the inclusive branching ratio is therefore about 43.5%.
- (3) **Fully hadronic.** The 4-jet decay mode occurs in 46.2% but it is unlikely to pass the L1 trigger thresholds without information from the FPDs. In addition the QCD background is expected to be overwhelming.

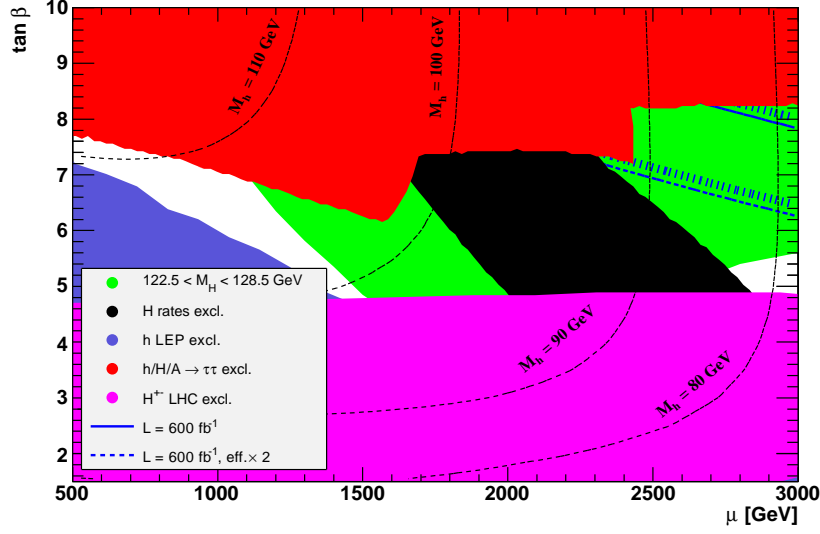


Fig. 2. Contours of 3σ statistical significance (solid blue lines) for the $h \rightarrow b\bar{b}$ channel in CEP at $\sqrt{s} = 14$ TeV in the $(\tan\beta, \mu)$ plane of the MSSM within the Low-MH benchmark scenario. The results are shown for assumed effective luminosities (see text, combining ATLAS and CMS) of 600 fb^{-1} and $600 \text{ fb}^{-1} \text{ eff} \times 2$. The values of the mass of the light \mathcal{CP} -even Higgs boson, M_h , are indicated by dashed (black) contour lines. The dark shaded (blue) region corresponds to the parameter region that is excluded by the LEP MSSM Higgs searches, the lighter shaded (red), the lighter shaded (pink) and black areas are excluded by LHC MSSM Higgs searches in the analyses of $h/H/A \rightarrow \tau\tau$, charged Higgs and Higgs rates, respectively. The light shaded (green) area corresponds to the allowed mass region $122.5 < M_H < 128.5$ GeV.

The backgrounds to the WW decay mode have been thoroughly discussed in Ref. 23 and also in Refs. 39, 40, 100. The main exclusive backgrounds can be divided into two broad groups: i) central production of a WW pair from the QED process $\gamma\gamma \rightarrow WW^{(*)}$ and ii) W -strahlung process arising from the QCD $gg \rightarrow Wq\bar{q}$ subprocess, where the (hadronically) decaying $W^{(*)}$ is faked by the two quarks. As shown in Ref. 39, 40 over a wide range of Higgs masses the photon-photon backgrounds can be strongly suppressed if the final state leptons and jets are required to be central and the cut $p_T > 200$ MeV on the proton transverse momentum measured in the FPDs is imposed. In general, the gluon-gluon QCD process with the W -strahlung is expected to be effectively suppressed by requiring the dijet mass to fall in an appropriate W mass window, since the background dijet mass distribution is a continuum beneath the W mass peak.¹⁰⁰ So for Higgs masses below the WW threshold (as in the case of the discovered Higgs boson with the measured mass of about 125 GeV) where the off-shell W -boson is the one decaying hadronically, and imposing a W mass window $70 < M_W < 90$ GeV on the measured dijet mass, one should effectively remove all events with hadronically decaying W^{*} -bosons and

enhance the signal-to-background ratio.

There are four analyses in the literature that deal with the $WW^{(*)}$ decay mode. In Ref. 40 the signal event yields for the fully leptonic and semileptonic channels are presented for the Higgs boson produced exclusively in the SM. In Ref. 39 the event yields are given for the Higgs bosons decaying semi-leptonically in the $\mu\nu jj$ final state and for its most important backgrounds, including the overlap source. Both these analyses concentrated on the mass point of 160 GeV where the cross-section is largest for this decay mode in the SM. On the other hand in Ref. 23 the main emphasis is on investigating prospects of the MSSM, in the vicinity of 120 GeV, because that is where the enhancement of MSSM over SM cross sections is largest (in the small α_{eff} scenario, giving a factor 4). A table of signal selection efficiencies in the range between 120 and 200 GeV has initially been provided in Ref. 15. In Refs. 23, 40 all important sources of irreducible background are discussed and ways to effectively suppress them experimentally are proposed. All analyses providing signal yields (Refs. 15, 39, 40) are based on the ExHuMe event generator. With similar FPD acceptances and signal selection cuts, analyses in Refs. 39, 40 arrive at similar signal event yields for a data taking period corresponding to an integrated luminosity of 30 fb^{-1} . According to Ref. 40 one expects to collect in total 2.3 and one Higgs boson decaying semi-leptonically and fully-leptonically, respectively, if all decay channels are included. Slightly less than one Higgs boson candidate with two W-bosons decaying semi-leptonically in the $\mu\nu jj$ final state is reported in Ref. 39. This can be viewed as a good agreement given the fact that all decay modes for each lepton contribute equally. The selection efficiencies presented in Ref. 15 are twice as high as those in Ref. 40, due to missing cuts suppressing the exclusive QED (the cut on p_T of outgoing protons) and QCD (mass window around the W-boson mass) backgrounds. Numerical estimates of the backgrounds are given in Ref. 39 for the semileptonic channel in the $\mu\nu jj$ final state. The exclusive QED $\gamma\gamma \rightarrow WW^{(*)}$ turned out to be the most important background but can be kept smaller than the signal yield thanks to the p_T cut on the proton measurements in FPDs. The overlap background turned out to be fully tamable after making use of the exclusivity cuts. These conclusions are valid for any instantaneous luminosity up to $10^{34} \text{ cm}^{-2} \text{ s}^{-1}$.

3.3. $H \rightarrow \tau\tau$

The Higgs boson branching ratio into two τ 's in SM at a mass of 120 GeV being ten times smaller than that into $b\bar{b}$ makes this decay mode less attractive than the other two discussed above. Similarly to the WW decay mode, there are three classes of events with respect to the decay mode of τ , namely the fully leptonic, semi-leptonic and fully hadronic, with a significant difference being the higher number of neutrinos in the final state. Important experimental advantages compared to the $b\bar{b}$ decay mode are i) the possibility of using high p_T lepton triggers and ii) that hadronic τ -jets have very low particle multiplicities, and are almost exactly back-to-back in azimuthal angle. The latter promises to enable us to effectively suppress

the overlap background even for the hadronic decays.

Backgrounds are discussed in Ref. 23. The dominant sources come from two processes: the QED $\gamma\gamma \rightarrow \tau\tau$ which can be safely neglected after applying cuts on the transverse momenta of the diffractive protons measured in the FPDs. The cut $p_T > 200$ MeV suppresses the QED background by a factor of 70, while the signal is reduced by 40%. The other important background comes from the CEP $gg \rightarrow gg$ where the outgoing gluons may mimic the tau. Imposing the same cut as in the $b\bar{b}$ case, $60^\circ < \theta < 120^\circ$, and assuming that the probability of misidentification of gluons to be tau, $P_{g/\tau}$ is smaller than 1/50, this source of background can be safely neglected. Note that in the inclusive events, thus in a less clean environment than in the exclusive case we are discussing here, $P_{g/\tau}$ has been evaluated to be $1/500^{101,102}$ and so our assumption is realistic.

Estimates of signal and background event yields for this decay mode have never been published. In Ref. 23, 24 the same signal selection efficiencies as for the $b\bar{b}$ decay mode are assumed, while the exclusive QED as well as QCD backgrounds have been properly calculated. Unpublished results¹⁰³ based on exclusivity cuts and including those suppressing both exclusive backgrounds discussed above confirm the similarity of the signal selection efficiencies between the $\tau\tau$ and $b\bar{b}$ modes. Prospects for this channel in MSSM have been presented in Refs. 23, 24 in the same benchmark scenarios as for the $b\bar{b}$ channel. Although the outlook for taming the overlap backgrounds is more favorable than for the $b\bar{b}$ decay mode, the significances are generally always lower.

4. Central Exclusive Higgs production in NMSSM

The Next-to-Minimal Supersymmetric Standard Model (NMSSM) extends the MSSM by introducing a singlet superfield. The Higgs sector in the NMSSM consists of three \mathcal{CP} -even and two \mathcal{CP} -odd neutral Higgs bosons and a charged Higgs boson. In this model the μ problem¹⁰⁴ can be solved and scale parameters do not need to be finely tuned as is the case in MSSM. However this is only possible if the lightest \mathcal{CP} -even Higgs boson h has a mass around 100 GeV and has SM couplings to gauge bosons and fermions. Consistency with LEP limits then results in h primarily decaying via $h \rightarrow aa \rightarrow \tau^+\tau^-\tau^+\tau^-$ where a is the lighter of the two pseudoscalar Higgs bosons present in the NMSSM. Both of these Higgs bosons might have escaped the LEP searches and they are almost impossible to detect at the LHC by standard tools. The troublesome low mass region may be covered by CEP. In Ref. 105 the above scenario is studied in detail with a scalar Higgs boson of mass 92.9 GeV decaying into two pseudo-scalar Higgs bosons a with masses of 9.73 GeV. The $h \rightarrow aa$ decay occurs in 92% cases and each a then decays into $\tau^+\tau^-$ with 81% probability. The analysis procedure is very similar to that used in studying the MSSM CEP $H \rightarrow b\bar{b}$ process in Ref. 22. The signal has been incorporated into the ExHuMe event generator, which also served to estimate the effect of irreducible backgrounds coming from the CEP $gg \rightarrow gg/b\bar{b}$ processes, and POMWIG was used to estimate

the DPE dijet background. The overlap background coming from pile-up events is treated as described in subsection 3.1.1. Finally the exclusive QED backgrounds $pp \rightarrow \tau^+ \tau^- l^+ l^-$ (where l is any charged lepton) were also considered and estimated using MADGRAPH.¹⁰⁶ The L1 trigger considered is a single muon with $p_T > 6$ GeV (which may have to be increased to 20 GeV at high luminosity).

After all cuts and using only the 420 FPD configuration (since the stations at 220 m do not contribute due to the low mass region of interest), effective cross sections (after applying all cuts) are 0.07 fb for signal and 0.002 fb for the non-overlap background, where the largest source is the DPE dijet production, while the QED source is entirely negligible. The overlap background is 0.005 fb at luminosities of $10^{34} \text{ cm}^{-2} \text{ s}^{-1}$ and 100 times lower at $10^{33} \text{ cm}^{-2} \text{ s}^{-1}$. These values correspond to a central mass window of 70–110 GeV assuming that such a wide interval will be needed when operating in a search mode. Once the signal is detected, a much narrower mass window can be applied thereby reducing the overlap background significantly. The small size of this background (compared e.g. to the CEP $H \rightarrow b\bar{b}$ channel where it represents a real challenge) is easily explained by a striking feature of the analysis adopted in Ref. 105 which relies on the tracking devices, FPDs and muon chambers, hence reducing the effect of calorimeters to a minimum. By selecting events with only 4 or 6 tracks and at least one muon with $p_T > 6$ GeV, of all combinations of four tau decays, only those are chosen where one tau decays to a muon whilst of the three remaining taus at most one of them is allowed to decay to three charged particles. By insisting also that the selected tracks have the right topology (they should cluster and form back-to-back pairs) we get a very favorable ratio of signal to overlap background: while 25% of signal is still available after the muon p_T cut, the overlap background is immensely suppressed.

The favorable signal-to-background ratio, and a signal event yield that is not extremely low, promises good prospects not only for measuring the mass of the scalar Higgs boson but also of the pseudoscalar a . Knowing the rapidity and mass of the central system from precise ξ -measurements at the FPDs, and assuming that the a 's are highly boosted (which would cause their decay products to follow roughly the direction of the parent τ 's), four a mass measurements per event are possible. With the efficiency of the muon trigger estimated to be around 50% and with the amount of data of 180 fb^{-1} collected at $3 \times 10^{33} \text{ cm}^{-2} \text{ s}^{-1}$, one can expect roughly 6 signal events with a negligible background, giving $m_a = 9.3 \pm 2.3$ GeV which is in a good agreement with the expected value of 9.7 GeV.

5. Central Exclusive Higgs production in Triplet Model

In SUSY models there are at least two Higgs doublets. Singlets occur in many extensions of the SM, see the previous section. In left-right symmetric models, triplets are added to generate a small mass for the neutrinos. The new scalars do not always participate in the electroweak symmetry breaking, nevertheless they affect the properties of the Higgs boson via mixing. Higgs triplets are used in models

such as composite Higgs or little Higgs. A tiny neutrino mass would indicate that the mass is generated by the seesaw mechanism which contains the couplings of neutrinos to the triplet. Ref. 28 shows that the lightest neutral Higgs boson of a model with triplets, H_1^0 , may be favorably searched for in CEP with proposed FPDs and at the same time, it identifies the representation of the found H_1^0 .

Since the studied Higgs boson decay is the $b\bar{b}$, the same analysis procedure applies as for the SM or MSSM CEP of $H \rightarrow b\bar{b}$ process (see Ref. 22). The only difference is in the cross section of the signal which in the triplet model is greatly enhanced with respect to SM: 113.5, 18.0 and 6.6 fb at $m_H = 120$ GeV for $c_H = 0.2, 0.5$ and 0.8 , respectively. The c_H is a parameter of the triplet model specifying the amount of the doublet-triplet mixing. At tree level, the coupling of the H_1^0 to fermions is always enhanced by a factor of $1/c_H$, while the gauge boson couplings to H_1^0 are suppressed by a factor of c_H with respect to the SM. Consequently the role of vector boson fusion for H_1^0 production is reduced if c_H is small. It was shown in Ref. 28 that for $c_H < 0.5$ the light Higgs boson H_1^0 (of mass between 120 and 150 GeV) can be observed with a significance of 4σ or better and its mass measurement can be made of better than 2 GeV resolution, if a fixed rate single jet trigger is used to retain events in which both protons are measured at 420 m from the IP.

6. Conclusions

Despite the achievements in terms of the discovery of the Higgs boson at LHC and measurements/estimates of its properties, the central exclusive production of the Higgs boson, whether of the SM or MSSM nature, still represents a powerful tool to complement the standard strategies at LHC. A striking feature of the CEP Higgs-boson is that this channel provides valuable additional information on the spin and the coupling structure of Higgs candidates at the LHC. We emphasize that the $J_z = 0$, \mathcal{C} -even, \mathcal{P} -even selection rule of the CEP process enables us to estimate very precisely (and event-by-event) the quantum numbers of any resonance produced via CEP.

In this review, the current status of the signal selection and of the background suppression for the CEP of Higgs bosons at LHC has been summarised, and numerous results have been collected and compared, where possible. The SM situation has been elaborated with a special attention since it represents a basis for all other analyses dealing with the New Physics to be searched for using the forward proton measurements. The significances for the CEP Higgs boson decaying into $b\bar{b}$, WW or $\tau\tau$ pairs in SM are moderate but 3σ can be reached if the analysis tools, ToF measurement resolution or L1 trigger strategies are improved. The fact that the mass 125.5 GeV Higgs boson is well known helps to optimize the strategy. Measurements and estimates made at LHC so far suggest the discovered Higgs boson is very consistent with the SM, hence room for New Physics at low masses is diminishing, while the high mass region still needs to be explored. In this review three models of New Physics have been examined, namely the MSSM, NMSSM and Triplet models.

The prospects of using central exclusive production to study this sector have been summarized, although upcoming results expected from the LHC Run II may change the outlook.

Acknowledgments

The work was supported by the project LG13009 of the Ministry of Education of the Czech republic. The author wishes to thank Valery Khoze for useful discussions, encouragement and assistance.

References

1. V.A. Khoze, A.D. Martin and M.G. Ryskin, *Eur. Phys. J. C* **14**, 525 (2000).
2. M. Albrow and A. Rostovtsev, arXiv:hep-ph/0009336.
3. V.A. Khoze, A.D. Martin and M.G. Ryskin, *Eur. Phys. J. C* **23**, 311 (2002).
4. M. Albrow, T. Coughlin and J. Forshaw, *Prog. Part. Nucl. Phys.* **65**, 149 (2010).
5. A. De Roeck, V.A. Khoze, A.D. Martin, R. Orava and M.G. Ryskin, *Eur. Phys. J. C* **25**, 391 (2002).
6. V.A. Khoze, A.D. Martin, M.G. Ryskin and A. Shuvaev, *Eur. Phys. J. C* **68**, 125 (2010).
7. L.A. Harland-Lang, V.A. Khoze, M.G. Ryskin and W.J. Stirling, arXiv:1301.2552 [hep-ph].
8. ATLAS Collab. (G. Aad *et al.*), *Phys. Lett. B* **716**, 1 (2012).
9. CMS Collab. (S. Chatrchyan *et al.*), *Phys. Lett. B* **716**, 30 (2012).
10. P. Bechtel, S. Heinemeyer, O. Stål, T. Stefaniak and G. Weiglein, arXiv:1403.1582 [hep-ph].
11. FP420 R&D Collab. (M. Albrow *et al.*), *JINST* **4**, T10001 (2009).
12. The AFP project in ATLAS, C. Royon, arXiv:1302.0623 [physics.ins-det]; M. Tasevsky, *Nucl. Phys. Proc. Suppl.* **179-180**, 187 (2008), ATL-PHYS-CONF-2008-019; R. Staszewski, arXiv:1104.1858 [physics.ins-det].
13. The CT-PPS upgrade project in CMS and Totem, M. Albrow, *AIP Conf. Proc.* **1523**, 320 (2012).
14. L.A. Harland-Lang, V.A. Khoze, M.G. Ryskin and W.J. Stirling, arXiv:1405.0018 [hep-ph].
15. CMS and TOTEM diffractive and forward physics working group, CERN/LHCC 2006-039/G-124, CMS Note 2007/002, TOTEM Note 06-5.
16. E. Chapon, C. Royon and O. Kepka, *Phys. Rev. D* **81**, 074003 (2010).
17. J. de Favereau de Jeneret *et al.*, arXiv:0908.2020 [hep-ph].
18. P. Bussey, T. Coughlin, J. Forshaw and A. Pilkington, *JHEP* **0611**, 027 (2006).
19. M. Tasevsky, arXiv:0910.5205 [hep-ph].
20. P. Lebiedowicz, R. Pasechnik and A. Szczurek, *Nucl Phys. B* **881**, 288 (2014).
21. A. Kaidalov, V.A. Khoze, A.D. Martin and M.G. Ryskin, *Eur. Phys. J. C* **33**, 261 (2004).
22. B. Cox, F. Loebinger and A. Pilkington, *JHEP* **0710**, 090 (2007).
23. S. Heinemeyer, V.A. Khoze, M.G. Ryskin, W.J. Stirling, M. Tasevsky and G. Weiglein, *Eur. Phys. J. C* **53**, 231 (2008).
24. S. Heinemeyer, V.A. Khoze, M.G. Ryskin, M. Tasevsky and G. Weiglein, *Eur. Phys. J. C* **71**, 1649 (2011).
25. M. Tasevsky, *Eur. Phys. J. C* **73**, 2672 (2013).

26. J. Forshaw *et al.*, *JHEP* **0804**, 090 (2008).
27. S. Heinemeyer *et al.*, arXiv:0811.4571 [hep-ph].
28. M. Chaichian, P. Hoyer, K. Huitu, V. A. Khoze and A. Pilkington, *JHEP* **0905**, 011 (2009).
29. S. Heinemeyer, V.A. Khoze, M.G. Ryskin, M. Tasevsky and G. Weiglein, arXiv:0909.4665 [hep-ph]; arXiv:1009.2680 [hep-ph].
30. S. Heinemeyer, V.A. Khoze, M.G. Ryskin, M. Tasevsky and G. Weiglein, arXiv:1106.3450 [hep-ph].
31. S. Heinemeyer, V.A. Khoze, M. Tasevsky and G. Weiglein, arXiv:1206.0183 [hep-ph].
32. J. Ellis, J. Lee and A. Pilaftsis, *Phys. Rev. D* **71**, 075007 (2005).
33. M. Carena, J. Ellis, A. Pilaftsis and C. Wagner, *Phys. Lett. B* **495**, 155 (2000).
34. H. Sun and C-X. Yue, *Eur. Phys. J. C* **74**, 2823 (2014).
35. M. Köksal, S.C. Inan, *Adv. High Energy Phys.* **2014**, 315826 (2014).
36. A. Senol, arXiv:1311.1370 [hep-ph].
37. M. Boonekamp, J. Cammin, S. Lavignac, R. Peschanski and C. Royon, *Phys. Rev. D* **73**, 115011 (2006).
38. M. Tasevsky, *AIP Conf. Proc.* **828**, 401 (2006).
39. A. Brandt, V. Juranek, A. Pal and M. Tasevsky, ATL-COM-PHYS-2010-337.
40. B.E. Cox *et al.*, *Eur. Phys. J. C* **45**, 401 (2006).
41. V.A. Khoze, A.D. Martin and M.G. Ryskin, *Eur. Phys. J. C* **19**, 477 (2001); Erratum-*ibid.* **C 20**, 599 (2001).
42. A.B. Kaidalov, V.A. Khoze, A.D. Martin and M.G. Ryskin, *Eur. Phys. J. C* **31**, 387 (2003).
43. M. Dührssen, S. Heinemeyer, H. Logan, D. Rainwater, G. Weiglein and D. Zeppenfeld, *Phys. Rev. D* **70**, 113009 (2004); arXiv:hep-ph/0407190.
44. R. Lafaye, T. Plehn, M. Rauch, D. Zerwas and M. Dührssen, *JHEP* **0908**, 009 (2009).
45. A. David *et al.* (LHC Higgs Cross Section Working Group), arXiv:1209.0040 [hep-ph].
46. S. Heinemeyer, C. Mariotti, G. Passarino and R. Tanaka (eds.) (LHC Higgs Cross Section Working Group), arXiv:1307.1347 [hep-ph].
47. A. Martin, M. Ryskin and G. Watt, *Eur. Phys. J. C* **66**, 163 (2010).
48. T. Coughlin and J. Forshaw, *JHEP* **1001**, 121 (2010).
49. V.A. Khoze, A.D. Martin and M.G. Ryskin, *Phys. Lett. B* **650**, 41 (2007).
50. V.A. Khoze, M.G. Ryskin and W.J. Stirling, *Eur. Phys. J. C* **48**, 477 (2006).
51. L. A. Harland-Lang, *Phys. Rev. D* **88**, no. 3, 034029 (2013).
52. R. Maciula, A. Szczurek and R. Pasechnik, *Phys. Rev. D* **83**, 114034 (2011).
53. R.A. Ryutin, *Eur. Phys. J. C* **73**, 2443 (2013).
54. V.A. Petrov and R.A. Ryutin, *J. Phys. G* **35**, 065004 (2008).
55. J.R. Cudell, A. Dechambre and O.F. Hernandez, *Phys. Lett. B* **706**, 333 (2012).
56. A.D. Martin, M.G. Ryskin and V.A. Khoze, *Acta Phys. Polon. B* **40**, 1841 (2009).
57. M.G. Ryskin, A.D. Martin and V.A. Khoze, *Eur. Phys. J. C* **60**, 265 (2009).
58. L.A. Harland-Lang, V.A. Khoze, M.G. Ryskin and W.J. Stirling, *Eur. Phys. J. C* **72**, 2110 (2012).
59. L.A. Harland-Lang, V.A. Khoze, M.G. Ryskin and W. J. Stirling, *Eur. Phys. J. C* **69**, 179 (2010).
60. J. Pumplin *et al.*, *JHEP* **0207**, 012 (2002).
61. T. Aaltonen *et al.* (CDF Collab.), *Phys. Rev. Lett.* **108**, 081801 (2012).
62. V.A. Khoze, A.D. Martin and M.D. Ryskin, *Eur. Phys. J. C* **55**, 363 (2008).
63. ATLAS Collab. (G. Aad *et al.*), arXiv:0901.0512 [hep-ex].
64. J. Monk and A. Pilkington, *Comput. Phys. Commun.* **175**, 232 (2006).
65. B.E. Cox and J.R. Forshaw, *Comput. Phys. Commun.* **144**, 104 (2002).

66. T. Sjostrand, S. Mrenna, P. Z. Skands, *JHEP* **0605**, 026 (2006); arXiv:0603175 [hep-ph].
67. G. Corcella *et al.*, arXiv:0201201 [hep-ph].
68. ATLAS Collab. (G. Aad *et al.*), ATLAS-CONF-2011-089.
69. CMS Collab. (S. Chatrchyan *et al.*), *J. Inst.* **8** P04013 (2013).
70. G. J. A. Brown *et al.*, ATL-DAQ-PUB-2009-006.
71. V.A. Khoze, A.D. Martin and M.G. Ryskin, *Eur. Phys. J. C* **60**, 249 (2009).
72. H. Nilles, *Phys. Rept.* **110**, 1 (1984).
73. H. Haber and G. Kane, *Phys. Rept.* **117**, 75 (1985).
74. R. Barbieri, *Riv. Nuovo Cim.* **11** 1, (1988).
75. M. Carena and H. Haber, *Prog. Part. Nucl. Phys.* **50**, 63 (2003).
76. S. Heinemeyer, *Int. J. Mod. Phys. A* **21**, 2659 (2006).
77. S. Heinemeyer, W. Hollik and G. Weiglein, *Phys. Rept.* **425**, 265 (2006).
78. M. Grothe *et al.*, CMS Note 2006/054 (2006), TOTEM NOTE 2006-01.
79. A.G. Shuvaev, V.A. Khoze, A.D. Martin and M.G. Ryskin, *Eur. Phys. J. C* **56**, 467 (2008).
80. V.A. Khoze, A.D. Martin and M.G. Ryskin, *Eur. Phys. J. C* **64**, 361 (2009).
81. S. Heinemeyer, W. Hollik and G. Weiglein, *Comp. Phys. Commun.* **124**, 76 (2000).
82. T. Hahn, S. Heinemeyer, W. Hollik, H. Rzehak and G. Weiglein, *Comp. Phys. Commun.* **180** (2009) 1426; see: www.feynhiggs.de.
83. S. Heinemeyer, W. Hollik and G. Weiglein, *Eur. Phys. J. C* **9**, 343 (1999).
84. G. Degrossi, S. Heinemeyer, W. Hollik, P. Slavich and G. Weiglein, *Eur. Phys. J. C* **28**, 133 (2003).
85. M. Frank, T. Hahn, S. Heinemeyer, W. Hollik, H. Rzehak and G. Weiglein, *JHEP* **0702**, 047 (2007).
86. P. Bechtle, O. Brein, S. Heinemeyer, G. Weiglein and K. Williams, *Comput. Phys. Commun.* **181**, 138 (2010); *Comput. Phys. Commun.* **182**, 2605 (2011).
87. P. Bechtle *et al.*, arXiv:1301.2345 [hep-ph]; arXiv:1311.0055 [hep-ph]; see: www.ippp.dur.ac.uk/HiggsBounds.
88. J. Ellis, S. Heinemeyer, K. Olive, A. Weber, G. Weiglein, *JHEP* **0708**, 083 (2007).
89. J. Ellis, T. Hahn, S. Heinemeyer, K. Olive and G. Weiglein, *JHEP* **0710**, 092 (2007).
90. G. Kribs, T. Plehn, M. Spannowsky and T. Tait, *Phys. Rev. D* **76**, 075016 (2007).
91. A. Djouadi and A. Lenz, *Phys. Lett. B* **715**, 310 (2012).
92. ATLAS Collab. (G. Aad *et al.*), ATLAS-CONF-2013-034.
93. CMS Collab. (S. Chatrchyan *et al.*), CMS-PAS-HIG-13-005.
94. ATLAS Collab. (G. Aad *et al.*), *Phys. Lett. B* **718**, 1284 (2013).
95. CMS Collab. (S. Chatrchyan *et al.*), *Phys. Lett. B* **718**, 307 (2012).
96. M. Carena, S. Heinemeyer, O. Stål, C.E.M. Wagner and G. Weiglein, *Eur. Phys. J. C* **73**, 2552 (2013).
97. T. Hahn *et al.*, arXiv:1404.0186 [hep-ph].
98. ATLAS Collab. (G. Aad *et al.*), ATLAS-CONF-2013-090.
99. V.A. Khoze, A.D. Martin and M.G. Ryskin, *Eur. Phys. J. C* **34**, 327 (2004).
100. V. A. Khoze, M. Ryskin and W. J. Stirling, *Eur. Phys. J. C* **44**, 227 (2005).
101. D. Cavalli *et al.*, ATLAS Internal note, PHYS-NO-051, 1994.
102. R. Kinnunen and A. Nikitenko, CMS Note 1997/002.
103. V. Kus, private communication. PhD thesis, 2014.
104. R. Dermisek and J. Gunion, *Phys. Rev. Lett.* **95**, 041801 (2005).
105. J.R. Forshaw *et al.*, *JHEP* **0804**, 090 (2008).
106. F. Maltoni and T. Stelzer, *JHEP* **02**, 027 (2003).